POLITECNICO
MILANO 1863

SCUOLA DI INGEGNERIA INDUSTRIALE
E DELL'INFORMAZIONE

Executive Summary of the Thesis

Characterization of a DECTRIS EIGER2 X CdTe 1M-W detector for medical imaging

Laurea Magistrale in Nuclear Engineering - Ingegneria Nucleare

Author: Camilla Giaccaglia

Advisor: Prof. Carlo Ettore Fiorini

Co-advisor: Dr. Luca Fardin

Academic year: 2021-2022

1. Introduction

Traditionally, advances in detector technology in the areas of high-energy physics, astronomy and medical imaging have stimulated the development of Synchrotron Radiation (SR) detectors. New opportunities for cross over to synchrotron studies arise with the most recent developments in these areas related to position- and energy-sensitive semiconductor detectors. This new type of detectors has shown great promise, due to their unique detection performances in terms of noise, dynamic range and readout speed. In 2019, the world leading developer and manufacturer of Hybrid Photon Counting (HPC) X-ray detectors, DECTRIS, has launched the EIGER2 X series for 4th generation synchrotron facilities. Their main applications include X-ray diffraction, X-ray scattering and spectroscopy. The ID17 beamline of the European Synchrotron Radiation Facility (ESRF), dedicated to biomedical research, purchased the EIGER2 X CdTe 1M-W for a different application: biomedical imaging, including Computed Tomography (CT) experiments and the K-Edge Subtraction (KES) technique. The goal of this thesis work was therefore to perform a detailed characterisation of the detector for this new application.

2. Material and Methods

The purpose of the characterization includes the determination of the performances of the detector in terms of linearity, Modulation Transfer Function (MTF), Noise Power Spectrum (NPS) and Detective Quantum Efficiency (DQE) and the determination of the detector stability at its startup and during a typical CT experiment. All the measurements were conducted at the biomedical beamline ID17. A detailed description of the beamline can be found in the publication of Elleaume et al. [1]. Briefly, the imaging end-station utilizes a monochromatic X-ray beam in the range 25-100 keV. Its location at about 150 m from the X-ray source provides a large beam (approximately 150×5 mm^2 (horizontal $\times$ vertical)) compatible with biomedical samples. The characterization of the detector was performed in the energy range 26-51 keV, typical of medical imaging experiments. Subsequently, some of the measurements were repeated at 80 keV, energy of interest for the K-edge of gold nano-particles. For the energy range 26-51 keV low and high conditions of flux have been tested, while for 80 keV, just low fluxes were studied to avoid the occurrence of the polarization phenomenon.

2.1. EIGER2

EIGER2 X CdTe 1M-X is a hybrid single photon counting detector, composed of two juxtaposed modules of 8 chips each one made of 256×256 pixels; the pixel size is 75×75 μm^2. The X-ray converter is a 0.75 mm thick Cadmium-Telluride (CdTe) crystal, determining a detection efficiency >60% in the energy range 25-60 keV with a flux up to 10^7 photons/pixel/s. It is based on a new Application Specific Integrated Circuit (ASIC), IBEX, developed by DECTRIS. IBEX offers an instant retrigger technology that yields non-paralyzable single-photon counting and improves high-rate counting performance. EIGER2 provides some automatic software corrections that can be enabled or disabled, including *flat-field*, for the correction of inter-pixel efficiency variability, and *count-rate* to compensate for counts loss at high photon fluxes. All these corrections have been applied in the experimental measurements presented below unless otherwise indicated.

2.2. EIGER2 performances

Linearity. The goal of the measurement was to verify a linear relationship between the number of counts of the detector and the incident photon flux. Once the linearity was verified, the influence of the count-rate correction on the detector output was studied. It was calculated at which flux the data, obtained by disabling the correction, deviated by more than 5% from the linear trend, providing a limit for the intrinsic linearity of the detector. Data were acquired in the energy range 26-51 keV and at 80 keV. The range of flux studied was: 5×10^6 photons/mm^2/s - 8×10^8 photons/mm^2/s. The incident photon flux was calculated by means of a calibrated PTW Semiflex TW31010 Ionisation Chamber (IC) (PTW, Freiburg, Germany) using a scanning technique developed at ID17 [2]: the small vertical angular divergence of synchrotron radiation hinders in fact the application of standard dosimetry protocols. The flux measured by the detector was determined by acquiring white-fields (wf), i.e. images of the beam, and by computing the mean number of counts, enabling and disabling the count-rate correction.
MTF. The MTF provides information on the spatial resolution of the detector and on its response to different spatial frequencies. The MTF was determined through the slanted-edge method [3]. Briefly, the image of a tungsten blade was acquired and the Edge Spread Function (ESF) was measured as the intensity profile across its edge. The blade was slightly tilted to sample the ESF with subpixel resolution. The ESF was differentiated to obtain the Line Spread Function (LSF). The MTF is defined as the Fourier amplitude of the LSF, normalized to one. Depending on the orientation of the edge, a vertical and a horizontal MTF can be measured. To improve numerical differentiation, a fit of the ESF is usually performed. In this work a new cutting-edge fit model for the ESF, developed by the Detector Group of the ESRF, was tested. It extends the typical sigmoid fit models found in literature by considering the physical dimension of the pixel and the effect of fluorescence photons on the spatial distribution of the charge released by the photon-sensor interaction. Fluorescence must be taken into account in the model as at the energies of 26.71 and 31.81 keV the K-edges of Cd and Te, respectively, are present. For those energies where the fluorescence is not present (<26 keV) or negligible (>60 keV), the model is given by the convolution of a Dirac delta (primary absorption), a Gaussian profile (charge diffusion), a box function (physical dimension of a pixel) and an edge response (slanted edge). The inclusion of fluorescence in the model leads to the superposition of a symmetric exponential to the Dirac delta, in order to account for the high distance charge tails from the primary photon impact point that fluorescence can give. Experimentally the MTFs were calculated for two flux conditions (low - 1M counts/pixel/s, high - 3M counts/pixel/s) for the energy range 26-50 keV, while for the energy of 80 keV just the low flux (1M counts/pixel/s) condition was studied. In particular, for each combination of energy-flux, both the horizontal and vertical MTF were studied. Insufficient statistics was obtained for the horizontal MTF, due to the limited vertical beam size; consequently only the results related to the vertical MTF will be presented.
NPS. The NPS describes the spectral decomposition of the variance in an image and the spatial correlation between pixels. It is computed from the modulus squared of the Fourier transform of a wf image. In this work the NPSs calculated

from 1000 wf were averaged to reduce the statistical uncertainty. The calculation of the NPS requires uniform irradiation of the detector, a condition not met by the gaussian intensity profile of synchrotron radiation. A detrend technique was therefore applied. As the detector shows a time dependent response during irradiation, the Savitzky-Golay denoise filter was used to estimate an instant-by-instant background correction. The same energy and flux conditions employed for the calculation of the MTF were used for the NPS. A Normalised NPS (NNPS) was calculated by multiplying the NPS for the incident photon fluence, determined with the PTW IC and normalizing it for the counts squared.
DQE. The DQE is defined as the output to input signal-to-noise-ratio squared. It is computed by dividing MTF and NNPS at each spatial frequency. Since only the vertical MTF was measured, only the vertical 1D profile of the DQE was computed.

2.3. EIGER2 stability

At startup. The stabilisation of the detector at the startup was studied to determine after how long the detector can be used following its initialisation by means of an High Voltage (HV) reset. 8 consecutive HV resets were performed, waiting one hour between one and the other. The measurement was performed without irradiation and by recording the leakage current of the detector with a sampling rate of one per minute.
During a CT scan. The purpose of this experiment was to verify whether the detector reaches stability during irradiation in a time compatible with a tomographic scan and to find out if repeated tomographic scans, a classical case of medical imaging experiment, were reproducible or not. Two different energies were tested, 33 keV and 50 keV, and for each energy two conditions of flux, low (about 150k counts/pixel/s) and high (about 1M counts/pixel/s). After 1 hour from a HV reset, the sensor was irradiated three times for 1 minute, simulating consecutive CT acquisitions (CT1, CT2, CT3), during which 1 wf image was acquired every 10 ms. A waiting time T_{sleep} in between irradiations simulated a dead time between consecutive tomographic scans. This protocol was repeated for each combination of energy, flux and varying T_{sleep}. Data were initially acquired at relatively low T_{sleep} times: 1 and 5 minutes, but in light of the results obtained, the dataset was enlarged for the energy of 33 keV to longer T_{sleep} times: 10 and 20 minutes.

3. Characterization Results

3.1. EIGER2 performances

Linearity. The results for the linearity analysis are summarized in Table 1, where the slope (m) and the intercept (q) for each energy are reported. The error associated with the intercept has not been indicated as it is compatible with zero. The linear fit was performed with ROOT (CERN).

E [keV]	m	q
26	(0.93±0.03)	0
28	(0.98±0.06)	0
30	(0.84±0.03)	0
35	(0.76±0.02)	0
51	(0.78±0.02)	0
80	(0.66±0.01)	0

Table 1: Slopes (m) and intercepts (q) of the linear fits for each energy studied.

When disabling the count-rate correction, a deviation greater than or equal to 5% from linearity was observed from a flux of approximately $3{\times}10^8$ photons/mm^2/s.
MTF. Table 2 shows the obtained results: for each condition of energy and flux the Full Width at Half Maximum (FWHM) of the LSF and the ESOP (Equivalent Size of Pixel) are reported. The latter figure of merit was introduced to quantify the frequency response alteration observed. It corresponds to the pixel size of an ideal perfect 2D detector that would present a similar MTF below the Nyquist spatial frequency as the detector under investigation [4]. To show the model output, in Figure 1 are reported the graphs related to the ESF, LSF and MTF for the energy of 33 keV at low flux, with the inclusion of the fluorescence in the model. In particular, to demonstrate the relevance of considering the fluorescence in the ESF fitting model, for those energies where the phenomenon occurs, both the graphs of ESF with and without the fluorescence are reported.

E [keV]	Flux [ph/mm^2/s]	FWHM [µm]	ESOP [µm]
26	1.58×10^8	74.79	78.87
	5.56×10^8	75.06	80.74
30	2.41×10^8	81.29	141.09
	6.99×10^8	78.29	135.53
33	2.02×10^8	77.55	141.11
	7.25×10^8	77.58	145.54
50	1.95×10^8	75.57	95.60
	6.58×10^8	75.58	94.51
80	3.98×10^7	74.86	78.56

Table 2: Final results for the MTF. The LSF FWHM and ESOP values are reported for each combination of energy and flux analysed.

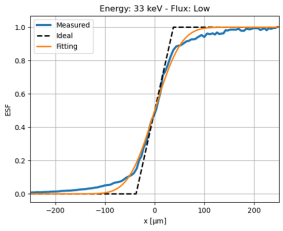

(a) ESF - no fluorescence

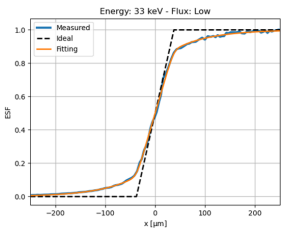

(b) ESF - fluorescence

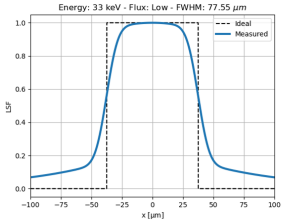

(c) LSF - fluorescence

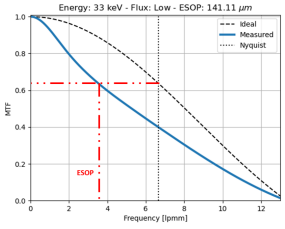

(d) MTF - fluorescence

Figure 1: MTF results for the energy of 33 keV at low flux. For each function the measured and the ideal curves are plotted. In addition, for the ESF the fitting model is reported while for the MTF the Nyquist frequency (6.67 mm^{-1}) is highlighted. The ESOP parameter is depicted.

NNPS. In Figure 2 the NNPS curves as a function of the spatial frequency for the energy range 26-80 keV, for low and high flux, are presented.
DQE. The DQE curves as a function of the spatial frequency for the energy range 26-80 keV and for each condition of flux are reported in Figure 3.

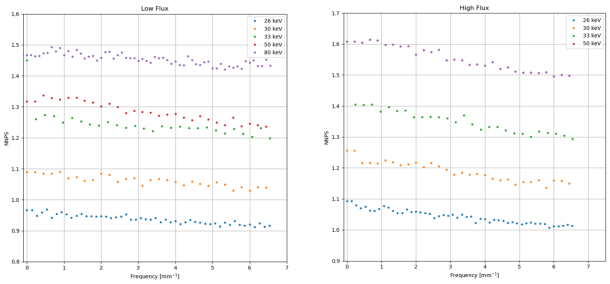

(a) (b)

Figure 2: NNPS as a function of the spatial frequency for the energy range 26-80 keV, at (a) low and (b) high flux.

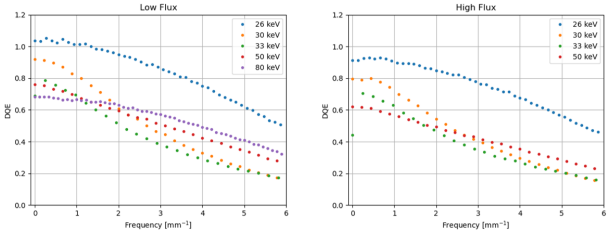

(a) (b)

Figure 3: DQE as a function of the spatial frequency for the energy range 26-80 keV, at (a) low and (b) high flux.

3.2. EIGER2 stability

At startup. Figure 4 shows the evolution of the leakage current after the 8 HV resets performed.

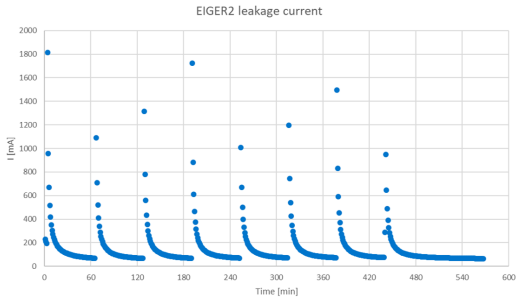

Figure 4: EIGER2 leakage current as a function of time acquired after each of the 8 HV resets performed 1 hour apart.

During a CT scan. In Figure 5 the main results for the energy of 33 keV and for each condition of flux, low and high, and T_{sleep} (1 and 5 minutes) are shown. In particular, the average counts of the wf normalized to the ring current acquired at the initial instant of irradiation of each CT are presented (CT1, CT2, CT3). A

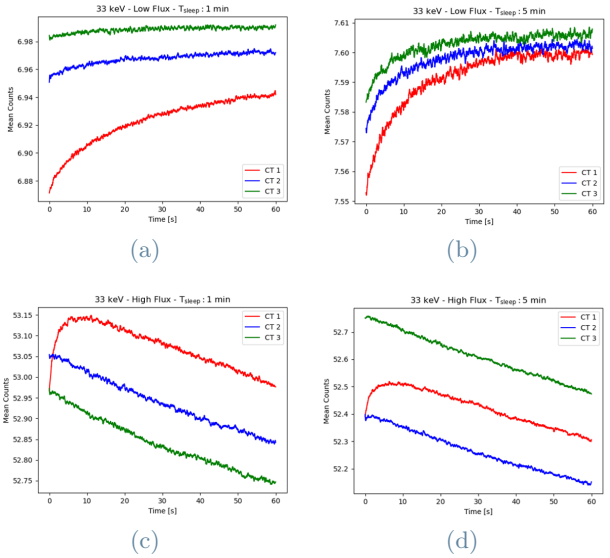

Figure 5: Normalized mean counts at 33 keV, for the low (a, b) and high (c, d) flux, and for the T_{sleep} time of 1 (a, c) and 5 (b, d) minutes. In red the first minute of irradiation (CT1), in blue (CT2) and green (CT3) the second and third minute of irradiation respectively.

smoothing of the data was performed through the application of the Savitzky-Golay filter.
In light of the results just presented, it was decided to see whether stable average counts correspond to a stable image. To study this, the ratio between the wf image at the end of the 1 minute irradiation for one CT and the wf image at time 0 (beginning of irradiation) for the same CT was performed. The calculation was done for each CT at each condition of flux and of T_{sleep} time. In Figure 6 the results at 33 keV, for the high flux condition and for both T_{sleep} times of 1 and 5 minutes are reported.

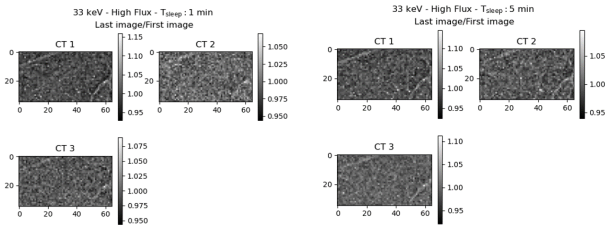

Figure 6: Images showing the ratio of the wf image acquired at the start of the irradiation minute to that acquired at the end of the irradiation minute for each CT. Results correspond to a photon energy of 33 keV, for high flux, and for T_{sleep} of (a) 1 and (b) 5 minutes.

4. Discussion

4.1. EIGER2 performances

Linearity. The linearity with count-rate correction enabled was verified for all energies. The angular coefficient of the linear relation is the efficiency of the detector. In light of the results reported in Table 1, it can be observed that around 30 keV a decrease in efficiency begins to occur. This deviation is attributable to the presence of the K-edges of Cd and Te. In fact, it may happens that fluorescence photons are absorbed by adjacent pixels. A recovery of efficiency is observed from 50 keV onwards, where the fluorescence phenomenon gradually diminishes. The efficiency decreases again at 80 keV. This behavior is in accordance with the measured and simulated quantum efficiency by DECTRIS, where around 30 keV and 80 keV a decrease is noted [5]. In the energy range 28-51 keV, the measurements obtained by enabling and disabling the count-rate correction differ more than 5% above an incoming flux of about $3{\times}10^8$ photons/mm^2/s.
MTF. For the MTF (refer to Table 2) a weak flux dependence has been observed and it has been noticed that, although the LSF gives a FWHM of about 75 µm for all the energies, a value reported by DECTRIS, the frequency response is completely altered, especially for those energies where the fluorescence contribution becomes important. In fact, for energies of 30 keV and 33 keV, where the fluorescence phenomenon is strong, the ESOP parameter is about twice as large as the ideal pixel size. Hence, it is more appropriate to consider the MTF than the LSF as the MTF gives a whole frequency characterization. As shown in Figure 1 the inclusion of the fluorescence in the model, for those energies for which the phenomenon occurs, leads to improved results, i.e. the fit is able to reproduce well the tails due to the fluorescence contribution.
NNPS. Concerning the NNPS results, shown in Figure 2, an almost ideal trend is obtained for low energies, i.e. NNPS about one (Poissonian statistical). At higher energies, the NNPS starts to degrade, probably due to a decrease in the

efficiency of the detector. Regarding the flux dependence, the NNPS data show a deviation from the ideal trend at higher fluxes for the same energy. Since the values corresponding to the high flux condition are higher than the value of 3×10^8 photons/mm^2/s for which the count-rate correction is seen to become preponderant, the degradation of the NNPS at high fluxes could be attributed to the fact that the detector is no longer locally linear and starts to deviate from the Poisson statistics.

DQE. DQE is a key performance parameter for digital X-ray detectors as it is a frequency dependent measure of the efficiency of the system in reproducing the information contained in the incident X-ray signal. As can be observed from Figure 3, for the energy range of 26-80 keV, a decrease of the DQE with energy for the same flux is verified. This behaviour is expected because as the energy increases, a loss of detector efficiency occurs, in agreement with DECTRIS' observations [5]. On the contrary, the decrease in DQE with flux is due to the behaviour of the NNPS. Contributing to this decrease of the DQE could also be a degradation of the output signal, probably due to the automatic corrections implemented by DECTRIS.

4.2. EIGER2 stability

At startup. The result in Figure 4 suggests that at least one hour must elapse after an HV reset before starting to acquire data. Furthermore, a repeatable trend of the current over time has been observed.

During a CT experiment. Figure 5 shows the trend of the normalized average counts over time for each minute of irradiation (CTs) for the energy of 33 keV and for relatively short T_{sleep} conditions, i.e. 1 and 5 minutes. This choice was made because the trend observed at 50 keV and for the other T_{sleep} times, is compatible with that reported. The trend of the curves obtained reflects the physics of the CdTe sensor. After the HV reset, all traps in the semiconductor material release almost all of the previously trapped charge. By irradiating the detector, there is a good chance that the created electrons will be trapped in deep states, which are characterised by trapping times of the order of minutes, if not hours. Hence, the initial increasing trend in counts for the first CT. For subsequent irradiations, this growth is only visible if longer T_{sleep} times, such as 10/20 minutes, are waited so as to allow time for the traps to release the previously trapped charge. For low fluxes a fairly stable zone is reached after about 30 seconds for all the CTs, while for higher fluxes a much more pronounced decrease is observed, which may be due to a slight onset of polarization. Globally the largest variation in the mean counts observed, for all the conditions analysed, is of the order of 1%. Thus, on average the detector can be considered stable at these energies. From the second analysis, the results of which were reported for the energy of 33 keV for the high flux (Figure 6), given the compatibility of the results for the other conditions studied, it was found that there are local variations in the pixel counts of the order of 5-6%. Locally the detector cannot be considered stable.

5. Conclusions

An extensive characterization has been made of the new EIGER2 detector purchased by the ID17 beamline, due to a lack of detector characterisation for biomedical imaging. Experimental measurements have shown that in view of medical imaging experiments it is advisable to operate at relatively low fluxes, in the order of 1M counts/pixel/s. At higher fluxes a degradation in NPS and DQE is observed. The global stability of the detector is compatible with CT experiments. The local variability may, however, affect image quality and quantitative measurements, such as KES results. The impact of these local instabilities on the specific ID17 imaging applications will be further investigated.

References

[1] H. Elleaume *et al.*, "Instrumentation of the ESRF Medical Imaging Facility," *Nucl. Instruments Methods Phys. Res. Sect. A: Accel. Spectrometers, Detect. and Assoc. Equip.*, vol. 428, no. 2-3, p. 513–527, 1999.

[2] Y. Prezado *et al.*, "Dosimetry Protocol for the forthcoming clinical trials in Synchrotron Stereotactic Radiation Therapy (SSRT)," *Med. Phys.*, vol. 38, no. 3, p. 1709–1717, 2011.

[3] Cunningham *et al.*, "A method for modulation transfer function determination from edge profiles with correction for finite-element differentiation," *Med. Phys.*, vol. 14, no. 4, p. 533–537, 1987.

[4] J. T. *et al.*, "Decimo: A simulation tool to explore next generation of detectors for synchrotron radiation applications," *IEEE*, pp. 1–7, 2016.

[5] DECTRIS, "EIGER2 X CdTe," 2018.